SUPPORTING MATERIAL

LIST S1 - List of PDB IDs of STY kinase complex structures retrieved from iPfam.

1B6C 1BI7 1BI8 1BLX 1BUH 1CKI 1CKJ 1CM8 1DS5 1E9H 1EH4 1F3M 1F5Q 1FIN
1FQ1 1FVV 1G3N 1GNG 1GY3 1H1P 1H1Q 1H1R 1H1S 1H24 1H25 1H26 1H27 1H28
1H4L 1H8F 1I09 1IAS 1J1B 1J1C 1J3H 1J91 1JKT 1JOW 1JST 1JSU 1JWH 1KOB 1KWP
1MRU 1NXK 1OB3 1OGU 1OI9 1OIU 1OIY 1OKV 1OKW 1OL1 1OL2 1OL5 1P5E 1PKD
1PYX 1Q3D 1Q3W 1Q41 1Q4L 1Q5K 1Q8Y 1Q8Z 1Q97 1Q99 1QMZ 1R0E 1S9I 1U5Q
1U5R 1UNG 1UNH 1UNL 1URC 1V0O 1V0P 1VYW 1W98 1WMK 1XO2 1Y8G 1YRP
1YXU 1Z9X 1ZMU 1ZMV 1ZMW 1ZWS 1ZXE 1ZY4 1ZY5 1ZYC 1ZYD 2A19 2A1A
2A27 2A2A 2BDW 2BFX 2BFY 2BKZ 2BMC 2BPM 2BUJ 2C47 2C4G 2C5N 2C5O 2C5V
2C5X 2C6T 2CCH 2CCI 2CJM 2CKE 2CLQ 2E9V 2EUF 2F2C 2F2U 2F49 2F57 2FA2
2FUM 2FYS 2G01 2G9X 2GCD 2GMX 2H34 2H96 2HAK 2HW6 2I0E 2I40 2I6L 2IW6
2IW8 2IW9 2IWI 2J4Z 2J50 2J90 2JAM 2JBP 2JD5 2JED 2JGZ 2JII 2JLD 2NO3 2NRU
2NRY 2O8Y 2OIB 2OIC 2OID 2OKR 2ONL 2OXY 2OZA 2PK9 2PMI 2PZY 2QCS 2QG5
2QNJ 2QVS 2R0I 2R7I 2R9S 2RIO 2UUE 2UZB 2UZD 2UZE 2UZL 2V22 2V55 2V5Q
2V62 2VD5 2VGO 2VGP 2VN9 2VRX 2VWB 2VWI 2VX3 2VZ6 2W96 2W99 2W9F
2W9Z 2WEV 2WFY 2WHB 2WIH 2WIP 2WMA 2WMB 2WNT 2WO6 2WPA 2WTK
2WTV 2WXV 2WZJ 2X0G 2X1N 2X4F 2X7F 2X7O 2XZS 2Y4I 2Y4P 2Y7J 2Y94 2YA9
2YAA 2YAB 2YDJ 2ZOQ 3A2C 3A60 3A7G 3A7H 3A8W 3A8X 3AG9 3AGL 3ALN
3ANQ 3ANR 3BEG 3BHH 3BHT 3BHU 3BHV 3BLH 3BLQ 3BLR 3C0G 3C0H 3C4E
3COH 3COK 3COM 3D0E 3DAE 3DAK 3DDP 3DDQ 3DLS 3DOG 3DS6 3DU8 3E3P
3E5A 3E7O 3E87 3E88 3E8C 3E8D 3E8E 3EB0 3EFW 3EID 3EJ1 3EN9 3ENH 3ENM
3EOC 3F5X 3F69 3F7Z 3FAA 3FBV 3FE3 3FHI 3FPQ 3FWQ 3G2F 3G33 3GC8 3GC9
3GCU 3GGF 3GNI 3GOK 3H0Z 3H10 3H30 3H4J 3H9R 3HA6 3HV4 3HV5 3HYH 3I4B

3I6U 3I6W 3IDB 3IDC 3IEC 3IS5 3IW4 3JUH 3KC3 3KCF 3KL8 3KN5 3KN6 3L1S 3LJ0 3LJ1 3LJ2 3LL6 3LQ5 3M1S 3MA6 3MDY 3MI9 3MIA 3MTF 3MVJ 3MVL 3MVM 3MY0 3MY1 3MY5 3N9X 3NAY 3NCZ 3NDM 3NIE 3NPC 3NR9 3O0G 3O17 3O2M 3O50 3O7L 3OCB 3OHT 3OP5 3ORI 3ORX 3ORZ 3OW4 3OZ6 3P23 3PUP 3PVB 3Q3B 3Q4T 3Q4U 3Q4Z 3Q9X 3Q9Z 3QA0 3QA8 3QC4 3QHR 3QHW 3R2B 3RAW 3RGF 3RNY 3SAY 3SD0 3SDJ 3SDM 3SLS 3SOC 3TAC 3TG1 3TL8 3TN8 3TNH 3TNI 3TNP 3TNQ 3TNW 3TV7 3UC4 3UDB 3UJG 3UNZ 3UO6 3UOH 3UOJ 3UOK 3UOL 3UYS 3UYT 3UZP 3V6R 3V6S 3V8S 3ZRK 3ZRL 3ZRM 3ZTX 3ZU7 3ZUT 3ZUU 3ZUV 4ACC 4ACD 4ACG 4ACH 4AE6 4AE9 4AF3 4AFJ 4AGU 4AOT 4APC 4ASX 4B8L 4BCF 4BCH 4BCI 4BCJ 4BCK 4BCM 4BCN 4BCO 4BCQ 4C02 4DFY 4DGL 4DIN 4EC8 4EC9 4EKK 4EOI 4EOJ 4EOK 4EOL 4EOM 4EON 4EOO 4EOP 4EOQ 4EOR 4EOS 4EUT 4EUU 4F6S 4F6U 4F6W 4F70 4F7J 4F7L 4F7N 4F7S 4F99 4F9A 4F9B 4F9C 4FX3 4FZA 4FZD 4FZF 4G6L 4I3Z 4IC7 4II5 4IMY 4IZ7 4IZA 4J7B

TABLE S1 – List of functional residues in the 55 STY kinases used in the study.

Numberings correspond to the residue numbers followed by the authors of the crystal structures available in the PDB

PDB ID	αC-helix	αG-helix	Activation loop				ATP binding loop	Hinge residues	Catalytic loop
			DFG motif	Activation segment	P+1 segment	APE motif			
1OL5_A	174-187	333-344	274-276	277-288	289-296	297-299	139-147	211-216	254-261
1OPL_A	299-311	463-474	400-402	403-414	415-425	426-428	267-275	335-340	380-387
2F4J_A	280-292	444-455	381-383	384-395	396-406	407-409	248-256	316-321	361-368
2GQG_A	280-292	444-455	381-383	384-395	396-406	407-409	248-256	316-321	361-368
2G2I_A	280-292	444-455	381-383	384-395	396-406	407-409	248-256	316-321	361-368
3DQW_A	304-316	467-478	404-406	407-418	419-429	430-432	273-281	339-344	384-391
2GS2_A	729-744	895-906	831-833	834-847	848-857	858-860	694-702	767-772	811-818
2ITP_A	753-768	919-930	855-857	858-871	872-881	882-884	718-726	791-796	835-842
1M14_A	729-744	895-906	831-833	834-847	848-857	858-860	694-702	767-772	811-818
1JBP_E	85-97	242-253	184-186	187-197	198-205	206-208	49-57	121-126	164-171
1APM_E	85-97	242-253	184-186	187-197	198-205	206-208	49-57	121-126	164-171
1L3R_E	85-97	242-253	184-186	187-197	198-205	206-208	49-57	121-126	164-171
1RDQ_E	85-97	242-253	184-186	187-197	198-205	206-208	49-57	121-126	164-171
2ERZ_E	85-97	242-253	184-186	187-197	198-205	206-208	49-57	121-126	164-171
2CPK_E	85-97	242-253	184-186	187-197	198-205	206-208	49-57	121-126	164-171
1FMO_E	85-97	242-253	184-186	187-197	198-205	206-208	49-57	121-126	164-171
1ATP_E	85-97	242-253	184-186	187-197	198-205	206-208	49-57	121-126	164-171
1IR3_A	1039-1052	1211-1222	1150-1152	1153-1168	1169-1176	1177-1179	1002-1010	1077-1082	1130-1137

1K3A_A	1013-1026	1187-1198	1123-1125	1126-1137	1138-1149	1150-1152	975-983	1050-1055	1103-1110
1PKG_A	631-647	874-886	810-812	813-825	826-836	837-839	595-603	671-676	790-797
1Y57_A	304-316	467-478	404-406	407-418	419-429	430-432	273-281	339-344	384-391
1W98_A	45-57	207-219	145-147	148-161	162-169	170-172	10-18	81-85	125-132
1QMZ_A	45-57	207-219	145-147	148-161	162-169	170-172	10-18	81-85	125-132
1FIN_A	45-57	207-219	145-147	148-161	162-169	170-172	10-18	81-85	125-132
1JST_A	45-57	207-219	145-147	148-161	162-169	170-172	10-18	81-85	125-132
3PY3_A	65-77	227-238	168-170	171-181	182-189	190-192	30-38	107-111	148-155
1NXK_A	99-111	267-281	207-209	210-216	227-230	231-233	70-78	139-144	184-191
2ERK_A	61-75	230-241	165-167	168-184	185-192	193-195	29-37	104-108	145-152
1YHW_A	309-321	468-480	407-409	410-423	424-431	432-434	276-284	345-350	387-394
3Q52_A	309-321	468-480	407-409	410-423	424-431	432-434	276-284	345-350	387-394
1YHV_A	309-321	468-480	407-409	410-423	424-431	432-434	276-284	345-350	387-394
1OL7_A	174-187	333-344	274-276	277-288	289-296	297-299	139-147	211-216	254-261
2FO0_A	299-311	463-474	400-402	403-414	415-425	426-428	267-275	335-340	380-387
2G1T_A	280-292	444-455	381-383	384-395	396-406	407-409	248-256	316-321	361-368
2HYY_A	280-292	444-455	381-383	384-395	396-406	407-409	248-256	316-321	361-368
2OIQ_A	304-316	467-478	404-406	407-418	419-429	430-432	273-281	339-344	384-391
3GOP_A	729-744	895-906	831-833	834-847	848-857	858-860	694-702	767-772	811-818
3GT8_A	729-744	895-906	831-833	834-847	848-857	858-860	694-702	767-772	811-818
2GS7_A	729-744	895-906	831-833	834-847	848-857	858-860	694-702	767-772	811-818
1XKK_A	753-768	919-930	855-857	858-871	872-881	882-884	718-726	791-796	835-842
4DFY_A	85-97	242-253	184-186	187-197	198-205	206-208	49-57	121-126	164-171

1SYK_A	85-97	242-253	184-186	187-197	198-205	206-208	49-57	121-126	164-171
2QVS_E	85-97	242-253	184-186	187-197	198-205	206-208	49-57	121-126	164-171
1IRK_A	1039-1052	1211-1222	1150-1152	1153-1168	1169-1176	1177-1179	1002-1010	1077-1082	1130-1137
1M7N_A	1039-1052	1211-1222	1150-1152	1153-1168	1169-1176	1177-1179	1002-1010	1077-1082	1130-1137
1T45_A	631-647	874-886	810-812	813-825	826-836	837-839	595-603	671-676	790-797
1FMK_A	304-316	467-478	404-406	407-418	419-429	430-432	273-281	339-344	384-391
2SRC_A	304-316	467-478	404-406	407-418	419-429	430-432	273-281	339-344	384-391
1HCL_A	45-57	207-219	145-147	148-161	162-169	170-172	10-18	81-85	125-132
1HCK_A	45-57	207-219	145-147	148-161	162-169	170-172	10-18	81-85	125-132
1P38_A	65-77	227-238	168-170	171-181	182-189	190-192	30-38	107-111	148-155
1NY3_A	99-111	267-281	207-209	210-216	227-230	231-233	70-78	139-144	184-191
1KWP_A	99-111	267-281	207-209	210-216	227-230	231-233	70-78	139-144	184-191
1ERK_A	61-75	230-241	165-167	168-184	185-192	193-195	29-37	104-108	145-152
1F3M_C	309-321	468-480	407-409	410-423	424-431	432-434	276-284	345-350	387-394

TABLE S2 - Matrix of ANOVA factors. Six parameters were considered: (i) Occupancy of the ATP binding site by ATP/ATP analog (1 if present, 0 if absent), (ii) Presence of bound substrate (1 if present, 0 if absent), (iii) Mutations in the kinase domain (1 if present, 0 if absent), (iv) Presence of bound cations near DFG loop (1 if present, 0 if absent), (v) Phosphorylation of a residue in the kinase domain (1 if present, 0 if absent) and (vi) Kinase (1 to 11 for the 11 kinases under study). The effect of the above said factors on the kinase functional state (1 if active, 0 if inactive) was analysed using Multi-factor Analysis of Variance (ANOVA)

PDB_ID	**ATP binding site occupied**	**Substrate peptide bound factor**	**Mutation in the kinase domain factor**	**Cation binding near DFG-loop factor**	**Phosphorylation in the kinase domain**	**Kinase**	**Kinase functional state**
1ATP_E	1	1	0	1	1	1	1
1OL5_A	1	0	0	1	1	2	1
1M14_A	0	0	0	0	0	3	1
1O6K_A	1	1	0	1	1	4	1
1JST_A	1	0	0	1	1	5	1
1PKG_A	1	0	0	1	0	6	1
1Y57_A	1	0	0	0	0	7	1
2ERK_A	0	0	0	0	1	8	1
1YHW_A	0	0	1	0	0	9	1
1IR3_A	1	1	0	1	0	10	1
1NXK_A	1	0	0	0	1	11	1
4DFY_A	0	0	1	0	0	1	0
1OL7_A	1	0	0	1	1	2	0
2GS7_A	1	0	1	1	0	3	0
1MRY_A	0	0	0	0	0	4	0
1HCK_A	1	0	0	1	0	5	0
1T45_A	0	0	0	0	0	6	0
2SRC_A	1	0	0	0	0	7	0

1ERK_A	0	0	0	0	0	8	0
1F3M_C	0	0	1	0	0	9	0
1IRK_A	0	0	0	0	0	10	0
1KWP_A	0	0	0	0	0	11	0

49

FIGURE S1 Investigation of effect of αC-helix conformation of the inactive state kinases on the structural fluctuations. Mean global mode NMS fluctuations of 31 active conformations listed in Table I (*blue curve*) and (A) 10 αC-helix-in inactive (*red curve*) and (B) 14 αC-helix-out inactive (*red curve*) conformations of STY kinase structures listed in Table III. The standard error of mean in the NMS fluctuations at each residue position is represented as shaded regions (*shaded blue* for active and *shaded red* for inactive). Residues are numbered arbitrarily from 1-361 irrespective of UniProt/PDB numbering. Green '*' symbol below the zero ordinate indicates significant difference between the distributions of active and inactive fluctuations of that residue. Structural and functional motifs in the kinase catalytic domain are marked below the zero ordinate. For regions of significant differential fluctuations, areas under the curves are plotted for (C) αC-helix-in inactive and αC-helix-out inactive conformations along with those for all the active and inactive conformations for comparison. The mean values for each of the distributions are also indicated.

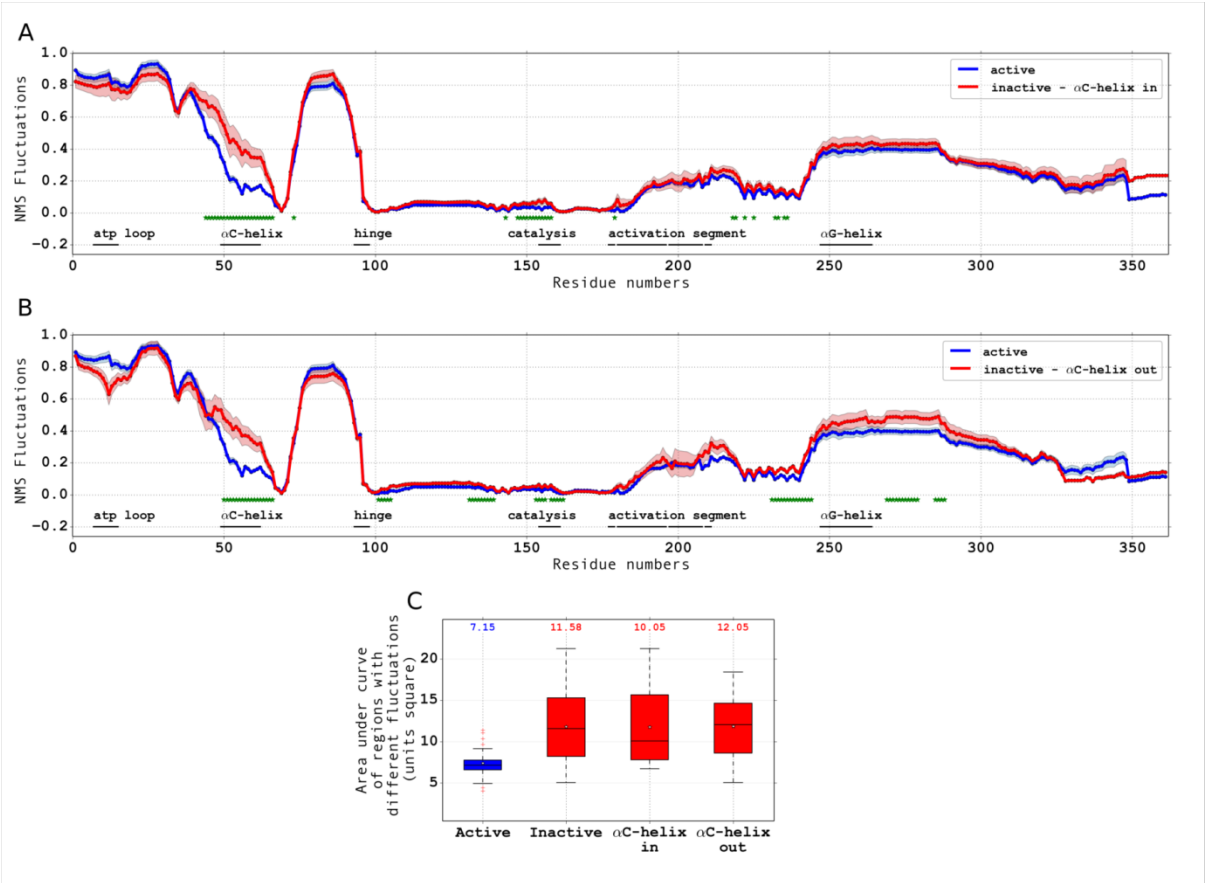

FIGURE S2 Investigation of effect of lobe closure conformation of the inactive state kinases on the structural fluctuations. Mean global mode NMS fluctuations of 31 active conformations listed in Table I (*blue curve*) and (A) 17 lobes-open inactive (*red curve*) and (B) 7 lobes-closed inactive (*red curve*) conformations of STY kinase structures listed in Table III. The standard error of mean in the NMS fluctuations at each residue position is represented as shaded regions (*shaded blue* for active and *shaded red* for inactive). Residue positions are numbered arbitrarily from 1-361. Green '*' symbol below the zero ordinate indicates significant difference between the distributions of active and inactive fluctuations of that residue. Structural and functional motifs in the kinase catalytic domain are marked below the zero ordinate. For regions of significant differential fluctuations, areas under the curves are plotted for (C) lobes-open inactive and lobes-closed inactive conformations along with those for all the active and inactive conformations for comparison. The mean values for each of the distributions are also indicated.

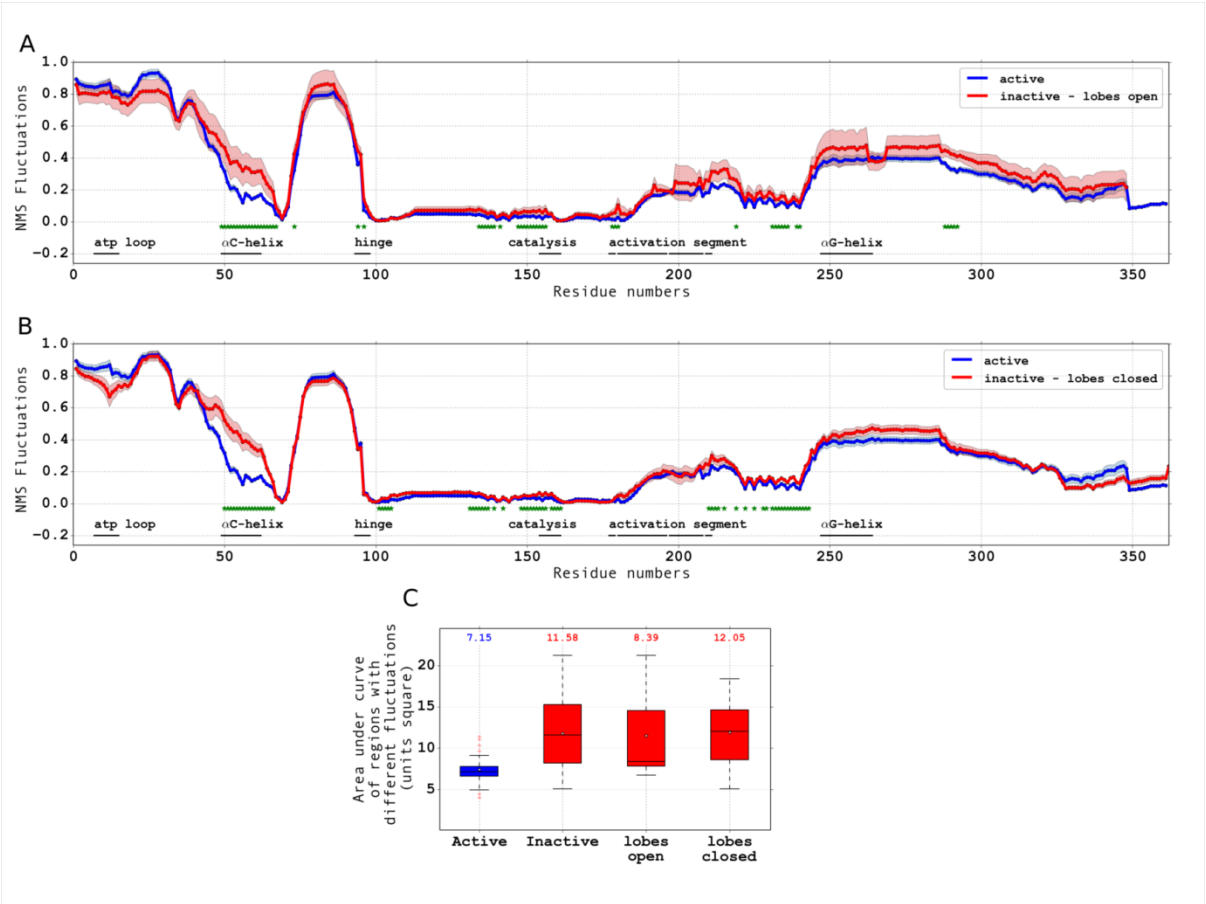

FIGURE S3 An all-atom example of GNM based NMA to investigate the effect of bound ATP analog on PKA. Two active conformation structures of PKA were chosen (holo form: 1FMO_E with bound ADP; apo form: 1APM_E without ATP or its analog). Network topology for the purpose of GNM was built using default parameters and all the atoms in the structures (including ADP atoms in case of the holo form). Global mode NMS fluctuations of the holo (*blue curve*) and the apo (*red curve*) forms are plotted. One can observe a reduction in fluctuation in the holo form near the ATP binding loop (*marked 'atp loop'*). However, no/minor change in fluctuation is observed in the regions of αC-helix, activation loop and αG-helix, which show high differential fluctuations between the active and inactive conformations.

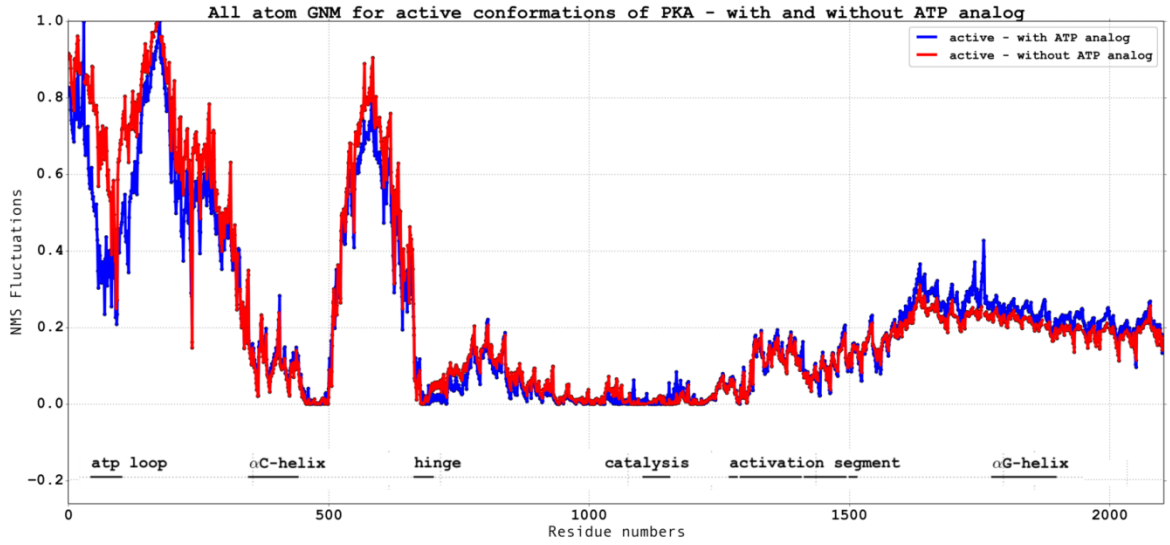

FIGURE S4 Structural deviation in the functional regions of active and inactive conformations of kinases. In order to understand the structural differences between the active and inactive conformations of STY kinases, we subjected 20 active-inactive conformation pairs (1OL5-1OL7, 2G2I-2G1T, 2G2I-2HYY, 1M14-3GOP, 1M14-3GT8, 1M14-2GS7, 1ATP-4DFY, 1ATP-1SYK, 1ATP-2QVS, 1IR3-1IRK, 1PKG-1T45, 1Y57-1FMK, 1Y57-2SRC, 1JST-1HCL, 1JST-1HCK, 3PY3-1P38, 1NXK-1NY3, 2ERK-1ERK, 1YHV-1F3M, 3DQW-2OIQ) to pairwise structural alignment usingTM-align[1]. (A) For each of the 20 pairs, residue-wise deviation in Å between the equivalent Cα atoms of the active and inactive conformations is plotted. (B) Mean deviation between equivalent Cα atoms of the active and inactive conformations across the 20 pairs is plotted (*blue solid line*) along with the standard error of mean (*shaded blue region*). It is seen that structural deviations are predominant in the activation segment, moderate in the ATP binding loop and αC-helix, minimum in the hinge, catalytic residues and α-helix.

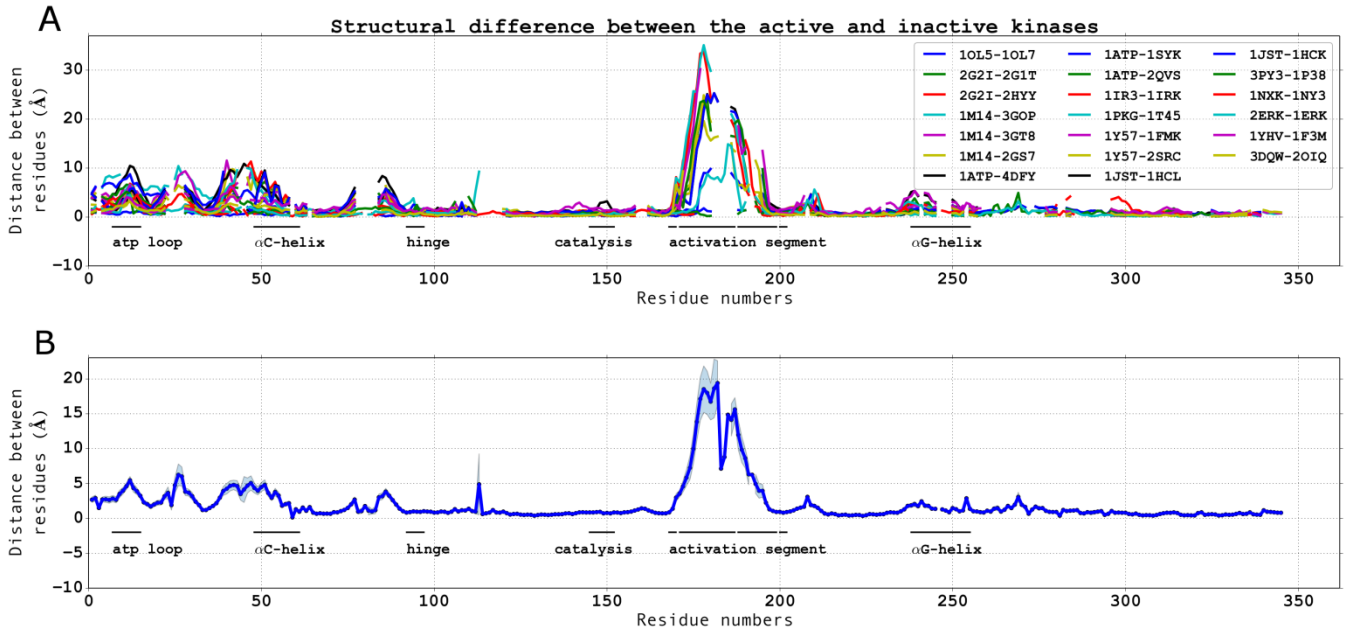

TABLE S3 Quantification of structural deviations in the functional regions. From the previous analysis (Fig. S5), structural deviations in the Cα atoms between the active and

106 inactive conformations were quantified for each of the functional regions of interest. As
107 observed previously, Cα atoms in the activation segment have an overall high deviation
108 between the active and inactive conformations. ATP binding loop and αC-helix also show
109 moderate structural deviation. However, regions like αG-helix and catalytic residues, which
110 showed up as having higher structural fluctuations in the inactive conformation than in the
111 active conformation, do not have significant deviations. In summary, although the magnitude
112 of structural deviations grossly corresponds to the difference in structural fluctuations, precise
113 relationship is sparse.

Region of interest	**residue nos. in PKA numbering (PDB_ID 1ATP_E)**	**RMSD in Cα atom positions across 20 pairs (Å)**	**Standard Error of Mean in Cα atom deviations across 20 pairs (Å)**
αC-helix	85-97	4.57	0.57
αG-helix	242-253	2.47	0.33
Activation segment	184-208	10.14	0.37
ATP binding loop	49-57	3.23	0.43
Hinge residues	121-126	1.04	0.12
Catalytic loop	164-171	0.94	0.10

114

115

FIGURE S5 Difference in distances across functional motifs between active and inactive conformations. For the 55 STY kinase structures considered for analysis in the study, all possible pair-wise distances were calculated between the centre residues of functional regions of interest. The functional regions of interest chosen were ATP binding loop (central residue according to PKA numbering : 53), αC-helix (91), hinge (124), catalytic residues (168), activation loop (196) and αG-helix (248). 15 distances were calculated for each of the 55 structures. Those pair-wise distances, whose distributions were statistically (two-tailed unpaired T-test, p-value < 0.05) different between the active and inactive structures are visualised in box plots. The distance (in Å) between functional regions of interest in active (*blue*) and inactive (*red*) structures are plotted, and the means are mentioned. It can be noted that all the inter-motif distances that were statistically distinct between the active and inactive conformations were the 5 distances calculated between αC-helix and other motifs. Also, in all the 5 cases, the inactive conformation distances are higher than the active conformation distances. This is likely a consequence of the outward movement of αC-helix ("out" conformation) in the inactive conformations. Interestingly, distances with respect to the activation loop did not statistically differ between the active and inactive states, in spite of prominent conformational change and structural deviation. This is probably because although the entire loop undergoes change, the central residue is unaltered in position. This way, the structural difference will not be reflected in this distance analysis.

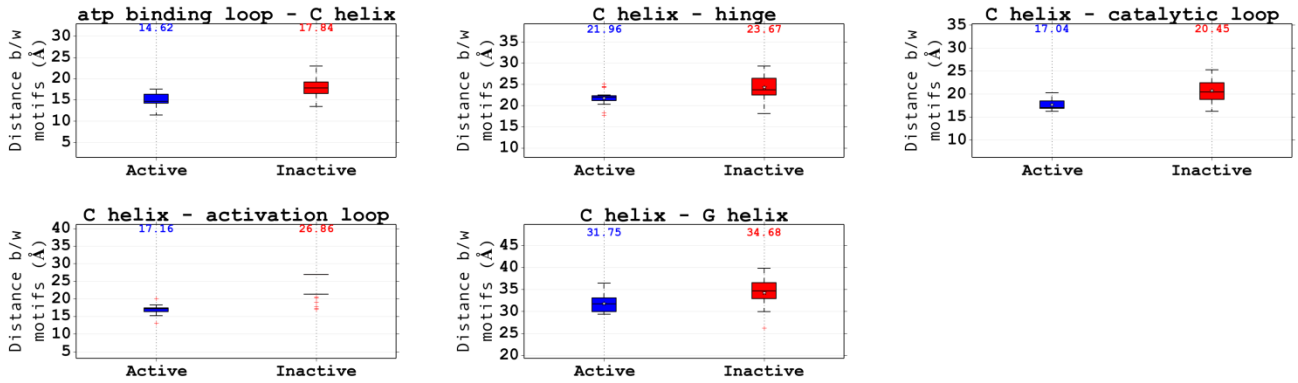

135

136 **TABLE S4 Mean and SEM of the inter-motif distances of the statistically different and**

137 **alike pairs.** For the 15 inter-motif pairwise distances analysed, we have tabulated the mean

138 and standard error of mean of the distributions across the active and inactive conformations.

139 See legend of Fig. S5 for details and interpretations.

Regions, between whose central residues, distance was calculated	**Mean of distances across 31 active conformations (Å)**	**Standard error of mean of distances across 31 active conformations (Å)**	**Mean of distances across 24 inactive conformations (Å)**	**Standard error of mean of distances across 24 inactive conformations (Å)**
With significantly (two-tailed unpaired T-test, *p*-value < 0.05) different distributions between active and inactive conformations				
ATP binding loop – αC helix	14.99	0.30	17.68	0.48
αC helix – hinge	21.73	0.33	24.29	0.55
αC helix – catalytic residues	17.68	0.20	20.77	0.52
αC helix – activation loop	16.90	0.20	22.83	1.07
αC helix – αG helix	31.77	0.34	34.22	0.59
Without significantly (two-tailed unpaired T-test, *p*-value > 0.05) different distributions between active and inactive conformations				
ATP binding loop - hinge	20.72	0.30	20.99	0.46
ATP binding loop – catalytic residues	16.05	0.40	16.86	0.76
ATP binding loop – activation loop	21.89	0.48	19.00	1.74
ATP binding loop – αG helix	27.36	0.53	28.41	0.80
Hinge – catalytic residues	17.92	0.16	18.15	0.22
Hinge – activation loop	33.90	0.32	33.07	1.31
Hinge – αG helix	37.56	0.26	37.76	0.42
Catalytic residues –	19.79	0.22	19.89	0.78

activation loop				
Catalytic loop – αG helix	20.28	0.17	20.32	0.33
Activation loop – αG helix	20.93	0.37	18.83	1.30

140

FIGURE S6 Difference in angles across functional motifs between active and inactive conformations. For the 55 STY kinase structures considered for analysis in the study, all possible inter-motif angles were calculated between the centre residues of functional regions of interest. The functional regions of interest chosen were the same as those chosen for the previous analysis. 20 angles were calculated for each of the 55 structures. Those inter-motif angles, whose distributions were statistically (two-tailed unpaired T-test, *p*-value < 0.05) different between the active and inactive structures are visualised in box plots. The angle (in degrees) between functional regions of interest in active (*blue*) and inactive (*red*) structures are plotted, and the means are mentioned. See Table S5 for a list of statistically different and alike quantified angles.

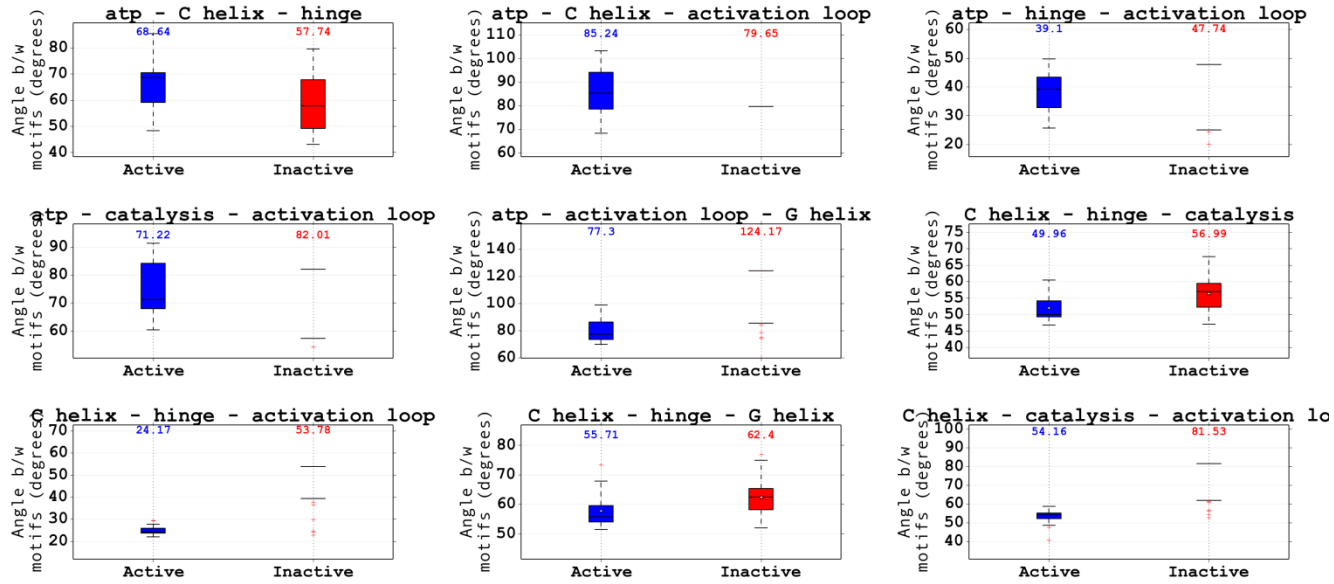

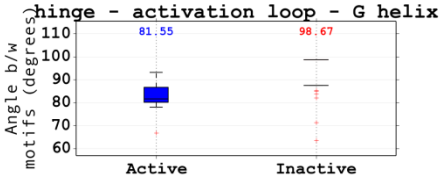

153 **TABLE S5 Mean and SEM of the inter-motif angles of the statistically different and**

154 **alike pairs.** For the 20 inter-motif angles analysed, we have tabulated the mean and standard

155 error of mean of the distributions across the active and inactive conformations. See legend of

156 Fig. S6 for details.

Regions, between whose central residues, angle was calculated	**Mean of angles across 31 active conformations (degrees)**	**Standard error of mean of angles across 31 active conformations (degrees)**	**Mean of angles across 24 inactive conformations (Å)**	**Standard error of mean of angles across 24 inactive conformations (Å)**
With significantly (two-tailed unpaired T-test, *p*-value < 0.05) different distributions between active and inactive conformations				
ATP binding loop – αC helix - hinge	66.19	1.68	58.26	2.10
ATP binding loop – αC helix – activation loop	85.99	1.73	54.23	6.65
ATP binding loop – hinge – activation loop	38.01	1.17	29.18	3.82
ATP binding loop – catalytic loop - activation loop	73.82	1.59	58.70	6.44
ATP binding loop – activation loop – αG helix	79.41	1.44	96.37	7.52
αC helix – hinge – catalytic loop	51.97	0.70	56.33	1.10
αC helix – hinge – activation loop	24.75	0.32	42.46	3.30
αC helix – hinge – αG helix	57.74	0.97	62.45	1.37
αC helix – catalytic loop – activation loop	53.26	0.61	68.49	3.23
Hinge – activation loop – αG helix	82.95	0.96	88.92	2.83
Without significantly (two-tailed unpaired T-test, *p*-value > 0.05) different distributions between active and inactive conformations				
ATP binding loop – αC helix – catalytic loop	58.16	1.71	52.45	3.42
ATP binding loop – αC helix – αG helix	58.84	1.74	56.34	3.29
ATP binding loop – hinge – catalytic loop	48.28	1.16	50.28	2.22
ATP binding loop – hinge – αG helix	45.31	1.42	47.42	2.48
ATP binding loop – catalytic loop – αG helix	97.12	1.72	98.59	2.26
αC helix – catalytic loop – αG helix	113.75	1.24	113.06	1.55
αC helix – activation loop – αG helix	113.37	1.41	112.13	4.18
hinge – catalytic loop – activation loop	128.00	1.00	122.46	4.42
Hinge - catalytic loop – αG helix	159.93	1.03	159.16	1.51
Catalytic loop – activation loop – αG helix	59.60	0.85	63.94	3.19

157

FIGURE S7 Difference in dihedral angles across functional motifs between active and inactive conformations. For the 55 STY kinase structures considered for analysis in the study, all possible inter-motif dihedral angles were calculated between the centre residues of functional regions of interest. The functional regions of interest chosen were the same as those chosen for the previous analyses (Refer Fig. S6). 15 dihedral angles were calculated for each of the 55 structures. Those inter-motif dihedral angles, whose distributions were statistically (two-tailed unpaired T-test, p-value < 0.05) different between the active and inactive structures are visualised in box plots. The dihedral angle (in degrees) between functional regions of interest in active (*blue*) and inactive (*red*) structures are plotted, and the means are mentioned. See Table S6 for a list of statistically different and alike quantified dihedral angles.

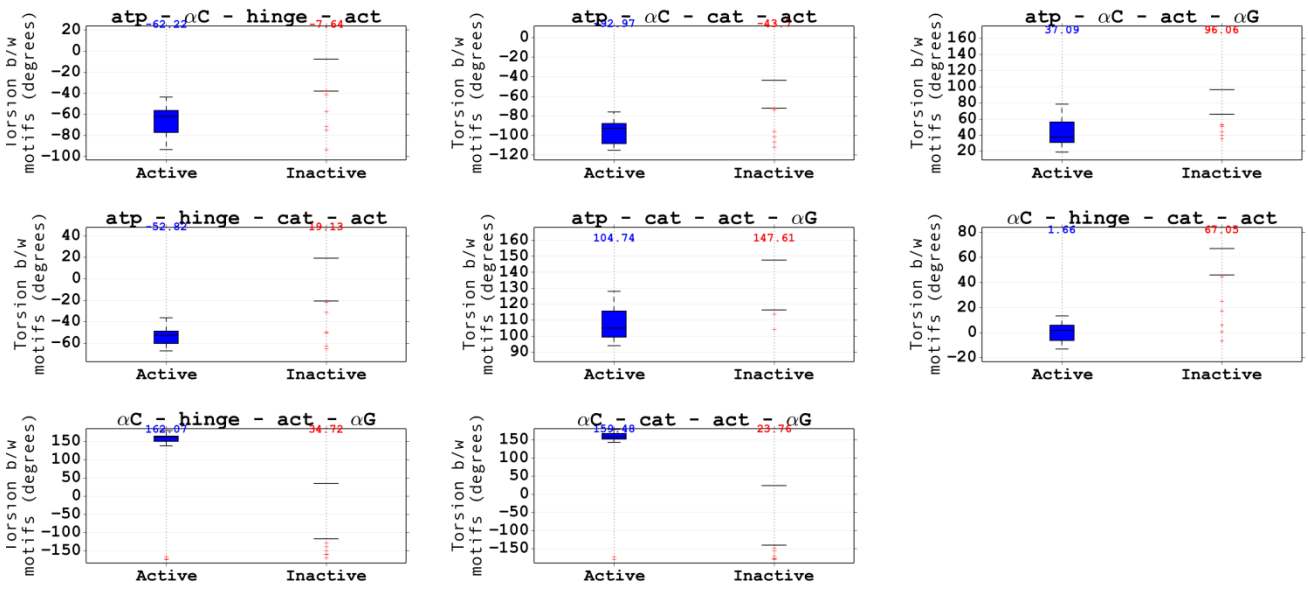

TABLE S6 Mean and SEM of the inter-motif dihedral angles of the statistically different and alike pairs. For the 15 inter-motif dihedral angles analysed, we have tabulated the mean and standard error of mean of the distributions across the active and inactive conformations. See legend of Fig. S7 for details.

Regions, between whose central residues, dihedral angle was calculated	**Mean of dihedral angles across 31 active conformations (degrees)**	**Standard error of mean of dihedral angles across 31 active conformations (degrees)**	**Mean of dihedral angles across 24 inactive conformations (Å)**	**Standard error of mean of dihedral angles across 24 inactive conformations (Å)**
With significantly (two-tailed unpaired T-test, *p*-value < 0.05) different distributions between active and inactive conformations				
ATP binding loop – αC helix – hinge – activation loop	-67.84	2.50	-34.99	7.69
ATP binding loop – αC helix – catalytic loop - activation loop	-97.93	2.10	-62.59	8.40
ATP binding loop – αC helix – activation loop – αG helix	40.27	2.79	76.49	9.51
ATP binding loop – hinge - catalytic loop - activation loop	-54.42	1.47	-13.12	8.26
ATP binding loop – catalytic loop - activation loop – αG helix	106.90	1.78	56.97	32.02
αC helix – hinge – catalytic loop – activation loop	0.06	1.34	43.71	6.90
αC helix – hinge – activation loop – αG helix	116.02	20.65	-67.98	30.84
αC helix – catalytic loop – activation loop - αG helix	137.66	15.43	-85.13	32.70
Without significantly (two-tailed unpaired T-test, *p*-value > 0.05) different distributions between active and inactive conformations				
ATP binding loop – αC helix – hinge - catalytic loop	-66.83	1.62	-65.02	3.23
ATP binding loop – αC helix – hinge - αG helix	-56.33	1.91	-55.11	3.58
ATP binding loop – αC helix - catalytic loop – αG helix	-79.30	2.06	-82.31	2.59
ATP binding loop – hinge – catalytic loop - αG helix	69.86	3.84	68.42	4.91
ATP binding loop – hinge – activation loop - αG helix	81.55	1.90	58.41	27.05
αC helix – hinge – catalytic loop - αG helix	123.28	3.32	109.09	12.38
hinge – catalytic loop – activation loop – αG helix	161.57	1.41	156.63	3.74

174

175

FIGURE S8 Domain motion prediction analysis using DynDom3[2,3]. Depicted below is an example superimposed cartoon representation of the active (*blue*, PDB_ID 1M14) and inactive (*grey*, PDB_ID 3GOP) Epidermal Growth Factor Receptor STY kinase. The arrow corresponds to the rotation vector about which the residues in the two lobes are predicted to move.

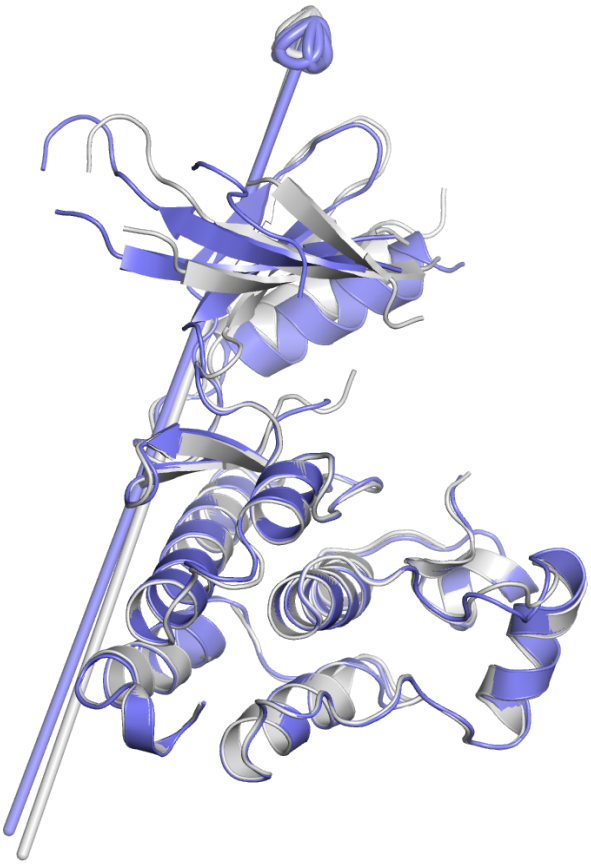

FIGURE S9 Effect of distance cut-off for topological constraint on the fluctuation differences. In order to test whether the distance cut-off used to build the network topology affected the main results of the study, we plotted the area under the curves of active (*blue*) and inactive (*red*) conformations' fluctuations as a function of cut-off value used. Although there are variations in the magnitude of difference between the active and inactive fluctuations, a similar trend of higher fluctuations in the inactive conformations than in the active conformations is observed throughout the range of cut-off values tested.

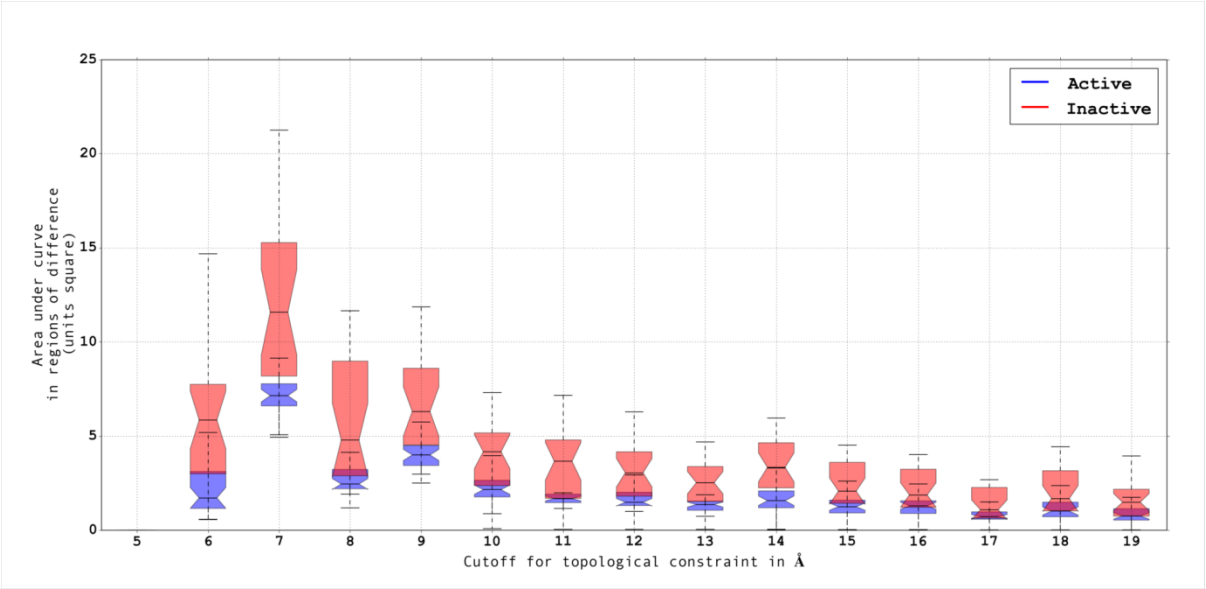

FIGURE S10 Correlation between the theoretically derived global mode NMS fluctuations and the experimentally determined B-factors. Global mode NMS fluctuations of the kinase catalytic domain residues is plotted with respect to the normalised B-factors of the corresponding residues for (A) active and (B) inactive structures used in the study.

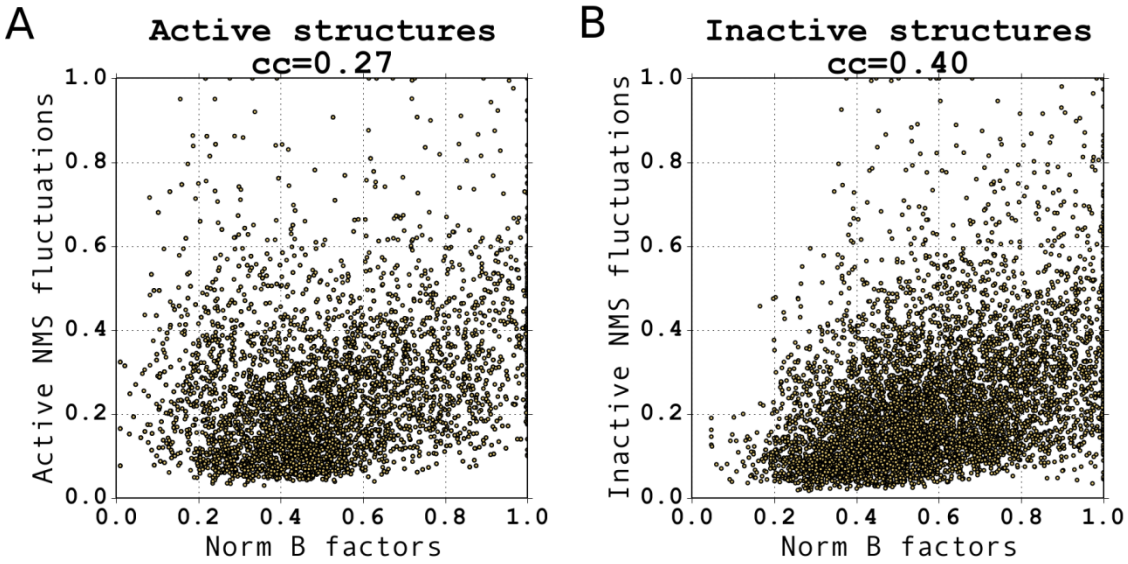

197 REFERENCES

198 1. Y. Zhang and J. Skolnick, *Nucleic Acids Res.*, 2005, **33**, 2302–9.

199 2. S. Hayward, A. Kitao and H. J. Berendsen, *Proteins*, 1997, **27**, 425–37.

200 3. G.P. Poornam, A. Matsumoto, H. Ishida and S. Hayward S. *Proteins,* 2009. **76,** 201-12

201